Available online at www.sciencedirect.com

ScienceDirect

J Materiomics 2 (2016) 114–130

www.ceramsoc.com/en/

www.journals.elsevier.com/journal-of-materiomics/

Band engineering and rational design of high-performance thermoelectric materials by first-principles

Lili Xi [a], Jiong Yang [b,**], Lihua Wu [b], Jihui Yang [c], Wenqing Zhang [b,*]

[a] State Key Laboratory of High Performance Ceramics and Superfine Microstructure, Shanghai Institute of Ceramics, Chinese Academy of Sciences, 1295 Dingxi Road, Shanghai 200050, China

[b] Materials Genome Institute, Shanghai University, 99 Shangda Road, Shanghai 200444, China

[c] Materials Science and Engineering Department, University of Washington, Seattle, WA 98195-2120, USA

Received 12 April 2016; accepted 8 May 2016
Available online 13 May 2016

Abstract

Understanding and manipulation of the band structure are important in designing high-performance thermoelectric (TE) materials. Our recent work has involved the utilization of band structure in various topics of TE research, i.e., the band convergence, the conductive network, dimensionality reduction by quantum effects, and high throughput material screening. In non-cubic chalcopyrite compounds, we revealed the relations between structural factors and band degeneracy, and a simple unity-η rule was proposed for selecting high performance diamond-like TE materials. Based on the deep understanding of the electrical and thermal transport, we identified the conductive network in filled skutterudites with the "phonon glass-electron crystal" (PGEC) paradigm, and extended this concept to caged-free Cu-based diamond-like compounds. By combining the band structure calculations and the Boltzmann transport theory, we conducted a high-throughput material screening in half-Heusler (HH) systems, and several promising compositions with high power factors were proposed out of a large composition collection. At last, we introduced the Rashba spin-splitting effect into thermoelectrics, and its influence on the electrical transport properties was discussed. This review demonstrated the importance of the microscopic perspectives for the optimization and design of novel TE materials.

Keywords: Thermoelectric materials; First-principles; Band engineering; Transport properties

Contents

* Corresponding author.
** Corresponding author.
E-mail addresses: jiongy@t.shu.edu.cn (J. Yang), wqzhang@t.shu.edu.cn (W. Zhang).
Peer review under responsibility of The Chinese Ceramic Society.

http://dx.doi.org/10.1016/j.jmat.2016.05.004

1. Introduction

In recent years, thermoelectrics has made a remarkable progress for its potentially broad applications in refrigeration, waste heat recovery, solar energy conversion, etc [1–7]. These solid state devices have no moving parts, are environmentally friendly, and are extremely reliable. The shortcoming of the existing thermoelectric (TE) materials is their relatively low energy conversion efficiency. The efficiency of TE materials depends on the dimensionless figure of merit $zT = S^2\sigma T/(\kappa_e + \kappa_L)$, where S is the Seebeck coefficient, σ is the electrical conductivity, T is the absolute temperature, and the thermal conductivity in denominator which can be divided to the electronic part κ_e and lattice part κ_L. Among those quantities, S, σ, and κ_e are related to the electronic structure of the material and κ_L is related to its phonon vibration. One possible way to optimize zT is to reduce the lattice thermal conductivity without significantly altering the electronic transport properties of the material. This strategy has been explored extensively by alloying, doping, and nano-composition [1,4,5] for the enhancement of phonon scattering. Another strategy is to maximize the power factor ($S^2\sigma$). This can be achieved by the band engineering and scattering engineering [8].

The band structures of materials describe the available energy levels for electrons, which are usually presented in the reciprocal space due to the periodicity of the lattice. The band structure is one of the basic characteristics of materials, as well as the vital tool in understanding, optimizing, and even designing novel functional materials. Since the electrical transport properties are directly determined by the band structures near the Fermi levels, the study of TE materials from the band structure perspective demonstrates as a model case which bridges the macroscopic electrical transport and the microscopic extremes of the materials. Explicitly, the power factor of the TE materials can be enhanced if one can manipulate the electronic density of states (DOS). This can be achieved by either band convergence as commonly accepted, or introducing new physical phenomena which alter the electronic structure [9–12]. In TE materials with complex structures, the electrical transport properties can be safely tuned if one can identify the conductive network as well as the out-of-network atoms of the materials, by electronic structure calculations. Combining with the Boltzmann transport theory, we can also use the band structures as the screening tools for predicting new TE materials with high power factors.

The three quantities like the Seebeck coefficient, electrical conductivity and electronic thermal conductivity are paradoxical, and the optimal power factor depends on the carrier concentrations. In degenerate semiconductors, the Seebeck coefficient under parabolic band approximation can be written as [13]:

$$S = \frac{8\pi^2 k_b^2 T}{3qh^2} m_d^* \left(\frac{\pi}{3n}\right)^{2/3}, \quad (1)$$

where m_d^* is the DOS effective mass, q the carrier charge, n the carrier concentration. Based on equation (1), a high S needs a high DOS (or m_d^*) at given Fermi level (carrier concentration). Since $m_d^* = N_v^{2/3} m_b^*$, where N_v is the band degeneracy and m_b^* is the band effective mass. There are two methods to increase the m_d^*, including increasing the effective mass of the single pocket m_b^* or the band degeneracy [14,15]. However, a high m_b^* always leads to a low carrier mobility due to their inversion relation. Band engineering, increasing the factor N_v without changing much of m_b^*, can effectively solve the paradox between the DOS effective mass and carrier mobility, and has been treated as an efficient strategy to improve TE performance [8,13,15,16]. Some excellent TE performance has been obtained by the band structure engineering. Through a distortion of the electronic DOS by doping Tl in PbTe, a doubling of zT in PbTe above 1.5 was obtained in 2008 [13]. By introducing multiple valley degeneracy, Pei et al. realized a high zT of 1.8 in doped $PbTe_{1-x}Se_x$ [15]. By solid solutions, band convergence was realized in $Mg_2Si_{0.35}Sn_{0.65}$, and a 65% improvement of power factor was obtained [17]. Tan et al. investigated the transport properties of Mn doped SnTe, and the results showed a high thermoelectric figure of merit of 1.3 at 900 K by the band modification [18]. Similar results were obtained by Pei et al. [19]. The band structure engineering mentioned above were caused by doping impurities in the framework. Besides these experiment results, some theoretical work also showed improved electrical transport properties by band convergence [9–12]. Recently, by tuning the structural parameters, Zhang et al. demonstrated a new strategy to achieve large band degeneracy that can predict and design high-performance non-cubic diamond-like TE materials, and the method can be used in layered compounds, such as Zintl compounds [20,21]. Besides, the Rashba spin splitting effect that can lead to lower-dimensional DOS and increase the S has been reported, which offers a new direction for electrical transport optimization [22–29].

It is critical for the improvement of TE materials to develop the corresponding novel concept and mechanism. Since the introduction of "Phonon glass-electron crystal" (PGEC) by Slack in 1995 [30], many TE materials with complex structures have been discovered, such as clathrates [31], skutterudites [32–36], zintl phases [37], diamond-like compounds [20], and liquid-like Cu_2Se or similar compounds etc [38]. Due to the various types of chemical bonds in complex compounds, and the fact that the electrical transport is determined by the band structures in a very small energy range, it is possible that only the fractions of the compounds dominate the electrical transport. This directly leads to the concept of the conductive network, with the in-network atoms constructing the "framework" and contributing to σ, and the out-of-network atoms acting as the carrier reservoirs. In some of the complex compounds, the out-of-network atoms, due to their loose bonding to the framework, their localized atomic motions can cause rattling modes in phonon spectra and reduce the κ_L. Our recent work on skutterudites and diamond-like compounds show that the TE performance can be improved by utilizing the conductive network, and this concept can be extended to other complex compounds [33,39–42].

The process of discovering new TE materials has been limited by the high cost and the time-consuming procedures of experiments. Recently, the computer-aided material design, especially the high-throughput material screening, brings up an avenue of material discovery. These work usually focus on the electrical transport properties, which are accomplished by the combination of band structure calculations and the Boltzmann transport theory under the relaxation time approximation. Yang et al. studied over 100 kinds of half-Heusler (HH) compounds based on high throughput calculations, and the work predicted a few HH compounds with potential high TE performance [43]. Their results are confirmed by recent experiments. By using high-throughput *ab initio* calculations, Wang et al. investigated more than 2500 sintered compounds from the Inorganic Crystal Structure Database (ICSD), and guided rules for searching for better TE materials, which are that sintered TE compounds with expected large power factors might have large band gaps, heavy carrier effective masses, and many atoms per primitive cell [44]. Carrete et al. investigated the TE performance of 75 nano-grained compounds out of 79,057 half-Heusler entries, and predicted that 15% of them might have high TE performance with $zT > 2$ at high temperatures [45]. Based on the high throughput computations from the Materials Project infrastructure, Zhu et al. screened 9000 materials and identified a new group of TE materials, i.e., trigonal and tetragonal $TmAgTe_2$, and a correlation between band degeneracy and maximum zT values was found [46]. Zhang et al. reported the orbital engineering strategy by solid solution map and biaxial strain engineering, which opens a new high-throughput computational screening in TE that can design high-performance TE materials from a myriad of non-cubic compounds [21]. The high-performance TE materials will be further discovered by the high-throughput methods.

In this paper, we summarize our theoretical work, regarding the electronic band structures and their applications in understanding, optimization, and design of TE materials. Some aspects deal with the band engineering, conductive network, and high-throughput calculation. The conclusion and further remarks are given at the end of the text.

2. Methods

All the calculations were carried out in projector augmented wave (PAW) method, as implemented in the Vienna *ab initio* Simulation Package (VASP). The Perdew-Burke-Ernzerhof generalized gradient approximation (GGA) for the exchange-correlation potential was used for most of the calculations [47–49]. The shortcoming of density functional theory (DFT) calculations is the underestimation of semiconductors' band gaps. However, for most TE materials, the band shape plays an important role in transport properties, and therefore localized density approximation (LDA) or GGA will be accurate enough when the temperature is below the onset of bipolar effects. The crystal structures of chalcopyrite semiconductors are relaxed using HSE06 functional [50]. The difficulty in treating these materials by *ab initio* calculations is the accurate description of d electron orbitals of copper, because the d orbitals of Cu are very close to the valence band maximum (VBM), and DFT + U methods have been widely used because they are simple yet powerful methods for correcting to some extent the problems with insufficient localization of d electrons. The value of the parameter U are used by a combined Wannier orbitals and constrained random phase approximation (cRPA) method that can refer to Y. B. Zhang's work [54]. So U = 4 eV was applied on Cu 3d states, Ag 4d states, Zn 3d states, and Cd 4d states [51–55]. Lattice constants were optimized by fitting the Birch–Murnaghan equation of state and ion positions are relaxed until the Hellmann-Feynman forces acting on each atom is less than 10^{-2} eV/Å. The details for other computation can be found elsewhere [20,43].

The Boltzmann transport theory can be used for studying electrical transport properties, including the Seebeck coefficients, electrical conductivity, and power factors. Under the relaxation time approximation, the time-evolution of distribution function follows $\left(\frac{\partial f}{\partial t}\right)_s = -\frac{f-f_0}{\tau}$, where f_0 and f are the equilibrium and perturbed carrier distribution functions, respectively, and τ is the relaxation time [56,57]. Based on this approximation, the electrical conductivity and the Seebeck coefficient tensors of a material can be written as [58,59].

$$\sigma_{\alpha\beta}(T,\mu) = \frac{1}{\Omega}\int \overline{\sigma}_{\alpha\beta}(\varepsilon)\left[-\frac{\partial f_0(T,\varepsilon,\mu)}{\partial\varepsilon}\right]d\varepsilon, \tag{2}$$

$$S_{\alpha\beta}(T,\mu) = \frac{1}{eT\Omega\sigma_{\alpha\beta}(T,\mu)}\int \overline{\sigma}_{\alpha\beta}(\varepsilon)(\varepsilon-\mu)\left[-\frac{\partial f_0(T,\varepsilon,\mu)}{\partial\varepsilon}\right]d\varepsilon, \tag{3}$$

where $\sigma_{\alpha\beta}(T,\mu)$,$\overline{\sigma}_{\alpha\beta}(\varepsilon)$ and $S_{\alpha\beta}(T,\mu)$ are tensor indices, Ω, μ, and f_0 are the volume of unit cell, Fermi level of carriers, and the carrier Fermi–Dirac distribution function, respectively, and e is the electron charge. The essential part of σ and S is the transport distribution function (TD) tensor defined as

$$\overline{\sigma}_{\alpha\beta} = \frac{e^2}{N}\sum_{i,\mathbf{k}} \tau_{i,\mathbf{k}}\cdot\nu_\alpha\cdot\nu_\beta\cdot\frac{\delta(\varepsilon-\varepsilon_{i,\mathbf{k}})}{d\varepsilon}, \tag{4}$$

where $\mathbf{k}$ and i are the wave vector and band index, respectively, and N is the number of $\mathbf{k}$ points sampled. The group velocity can be derived directly from the band structure by $\mathbf{v}_{i,\mathbf{k}} = \frac{1}{\hbar}\nabla_{\mathbf{k}}\varepsilon_{i,\mathbf{k}}$, where the $\varepsilon_{i,\mathbf{k}}$ is the band energy of indexed band i at $\mathbf{k}$ point, and the other method via the momentum matrix elements is defined as $\mathbf{v}_{i,\mathbf{k}} = \frac{1}{m_e}\mathbf{\Psi}_{i,\mathbf{k}}|\widehat{\mathbf{p}}|\mathbf{\Psi}_{i,\mathbf{k}}$, where m_e is the mass of electron, and $\mathbf{\Psi}_{i,\,k}$ is the wave function. The methods both are suitable for structures with small unit cells, such as half-Heusler compounds [43,59–66]. However, the direct method based on the gradients of the band energy is not applicable to systems with large unit cells due to the band-crossing problems [57,59]. The electrical transport properties of some materials were reviewed [20,42,43], since the complex unit cells needed for cases such as doping, are

evaluated by the momentum matrix method with the code Transoptic [67].

The relaxation time is affected by many scattering mechanisms, most of which are difficult to calculate. Fortunately, for TE materials without extremely sharp band structure features [68], constant relaxation time approximation can provide the Seebeck coefficients that are close to the experimental values. The constant relaxation time approximation has been employed by several groups when evaluating the electrical transport properties of thermoelectric compounds [57–63]. For the study of series of TE compounds with the same crystal structures and the similar chemical compositions, the relative magnitude of σ/τ and $S^2\sigma/\tau$ and their temperature dependence are also useful for the related experiments. In this paper, we mainly deal with on the band structure-oriented work.

3. High-performance materials by band engineering

3.1. Manipulating the structure–property relation—band degeneracy of pseudocubic structure materials

Band degeneracy is one of widely used approaches of band engineering, which include the orbital degeneracy (band degeneracy at one extrema point) and valley degeneracy (separate pockets at the same or similar energy). Highly degenerated bands indicate enhancement of m_d^* through increasing N_v, and therefore the Seebeck coefficient without significantly decreasing the electrical conductivity. In most of the work, however, the dopants or compositions favorable to large band degeneracies are found more or less by luck. So far, there is no systematic work that is able to provide criteria leading to the band convergence. In this subsection, we demonstrate the approach of rationally tuning crystal structures to design pseudocubic or cubic-like structural blocks in non-cubic diamond-like materials that can cause cubic-like degenerate valence band [20]. A simple unity-η rule was then proposed to design high PF and zT values for pseudocubic diamond-like compounds, and the details can be found elsewhere [20].

The diamond-like ternary and quaternary chalcopyrite compounds always have the distorted tetragonal structure. The cation sublattice can be tuned to show cubic or nearly cubic framework, while the anion sublattice shows a locally distorted non-cubic framework with two types of irregular tetrahedra in ternary chalcopyrites, leading to a periodic supercell with a cubic framework (see Fig. 1(a)). They actually have a doubled unit cell in the z-direction. In contrast to the zinc blende lattice, the triply degenerate valence band Γ_{5v} in tetragonal chalcopyrites will split into a non-degenerate band Γ_{4v} and a doubly degenerate band Γ_{5v} (see Fig. 1(b)), due to the crystal field effect [69,70]. The energy difference between Γ_{5v} and Γ_{4v} is defined as the crystal field splitting energy $\Delta_{CF} = E(\Gamma_{5v}) - E(\Gamma_{4v})$, which is positive when Γ_{5v} is above Γ_{4v} and negative in the opposite case. By systematically studying the connection between transport properties and electronic structures, we found that TE performance is closely related to the band degeneracy. zT values [34,71–77] at 700 K in non-cubic tetragonal chalcopyrites with calculated Δ_{CF} values are shown in Fig 1(c). High TE performance with the zT values enhances (see below for details) in noncubic tetragonal chalcopyrites [34,71–77] for $\Delta_{CF} = 0$. The absolute value of Δ_{CF} ($|\Delta_{CF}|$) could thus be considered as a parameter indicating the deviation from pseudocubic or cubic-like degenerate electronic bands of tetragonal chalcopyrite compounds.

The results of our study indicates that the Δ_{CF} has a strong dependence with the structural parameter η defined as $\eta = c/2a$, where a and c are lattice parameters (see Fig. 1(b)). $\Delta_{CF} \approx 0$ corresponds to an ideal value of $\eta \approx 1$. The above results present a simple but insightful knowledge that TE transport properties should show the same trend as a function of η as they do as a function of Δ_{CF}. Hence, promising TE

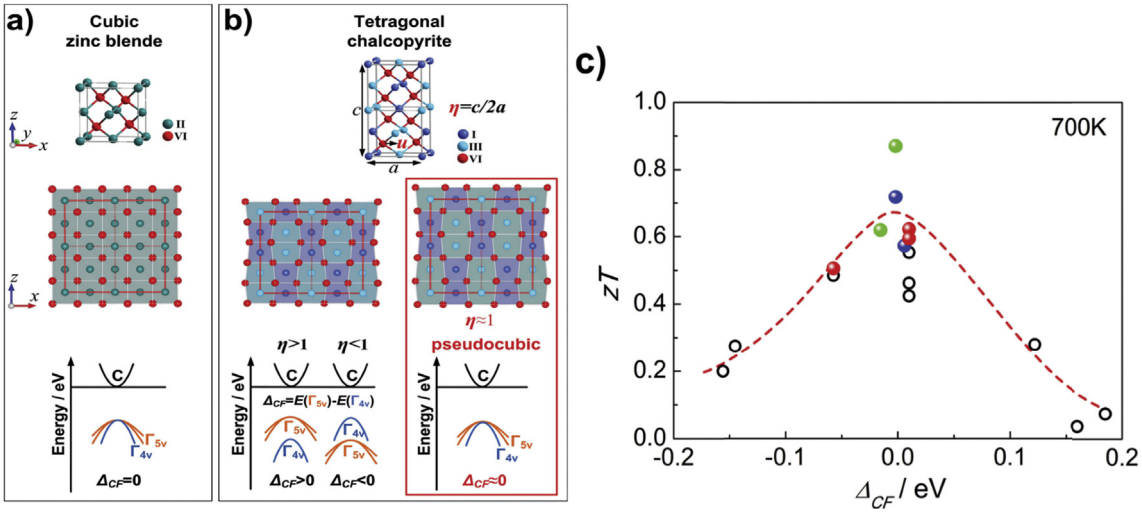

Fig. 1. Pseudocubic approach to realize highly degenerate electronic bands that yield good electronic-transport properties and a high thermoelectric figure of merit zT in non-cubic chalcopyrites. (a) Crystal structure and electronic bands of cubic zinc blende structure. (b) Crystal structure and electronic bands of ternary chalcopyrites. (c) zT values [34,71–78] at 700 K in non-cubic tetragonal chalcopyrites with calculated Δ_{CF} values [20].

materials, chalcopyrites should have a tetragonal distortion parameter around unity—the unity-η rule.

The unity-η rule provides a strategy of guiding the evaluation and optimization for TE chalcopyrites. Since the parameter η can be easily obtained from lattice parameters *a* and *c*, the unity-η rule can be straightforwardly applied to the evaluation of TE performance of all tetragonal chalcopyrites. The unity-η rule can be also extended to the design of novel pseudocubic multinary high-performance TE chalcopyrites. Fig. 2(a) shows that the cubic-like cation framework can be maintained in solid solutions or mixed multinary chalcopyrites, although the simulation indicates that there are a variety of tetrahedra with arbitrary deformation and different anion displacements due to nearly random distribution of the anions. Similarly, cubic-like valence band edges are observed as a result of symmetry operations on the cubic framework in supercells (see Fig. 2(b)). Taking $Cu_{0.875}Ag_{0.125}InTe_2$ as an example, the valence bands at Ã point are highly degenerated, implying an ideal character of pseudocubic structures (see Fig. 1). Fig. 2(c) shows the *η vs. a* dependence for chalcopyrite compounds where *a* is the lattice constant. Only the systems with bandgaps <1.7 eV are shown out of a myriad of chalcopyrite compounds. The pseudocubic approach with the aid of the unity-η rule, is very effective in screening prospective solid solutions and mixtures of chalcopyrite compounds. As the overall objective is to maintain an ideal value of $\eta = 1$, one may select a few compounds with higher (>1) and lower (<1) η values and reasonable lattice mismatch and attempt to form a solid solution or mixed state with $\eta \approx 1$ by appropriately varying the molar ratio of the two constituent compounds (see Fig. 2(c)). Experimentally, the $CuIn_{1-x}Ga_xTe_2$ and $Cu_{1-x}Ag_xInTe_2$ were synthetized and the performance are shown in Fig. 2(d). From the Ref. [15], Fig. S4, S5 and S6, we can see that the enhanced *zT* value are mainly due to the power factor improvement other than the thermal conductivity reduction by solid solutions [20]. So the much enhanced *zT* values than single chalcopyrite compounds are consistent with the theoretical predictions.

In this subsection, we demonstrate a new strategy to design high-performance non-cubic TE materials through the utilization of a rational pseudocubic structure that results in cubic-like degenerate electronic bands. We identify a simple yet powerful selection rule based on maintaining the distortion parameter η near unity, and which is shown to be equivalent to minimizing the energy-splitting parameter $Ä_{CF}$. Using this approach, we predicted a series of highly efficient chalcopyrite TE materials and, on a selected subset of them, we verify experimentally that they indeed possess significantly enhanced *zT* values. The approach can be further applied to other tetragonal semiconductors as well as other non-cubic materials in order to achieve cubic-like degenerate electronic bands. This work thus addresses the interest of researchers to broaden

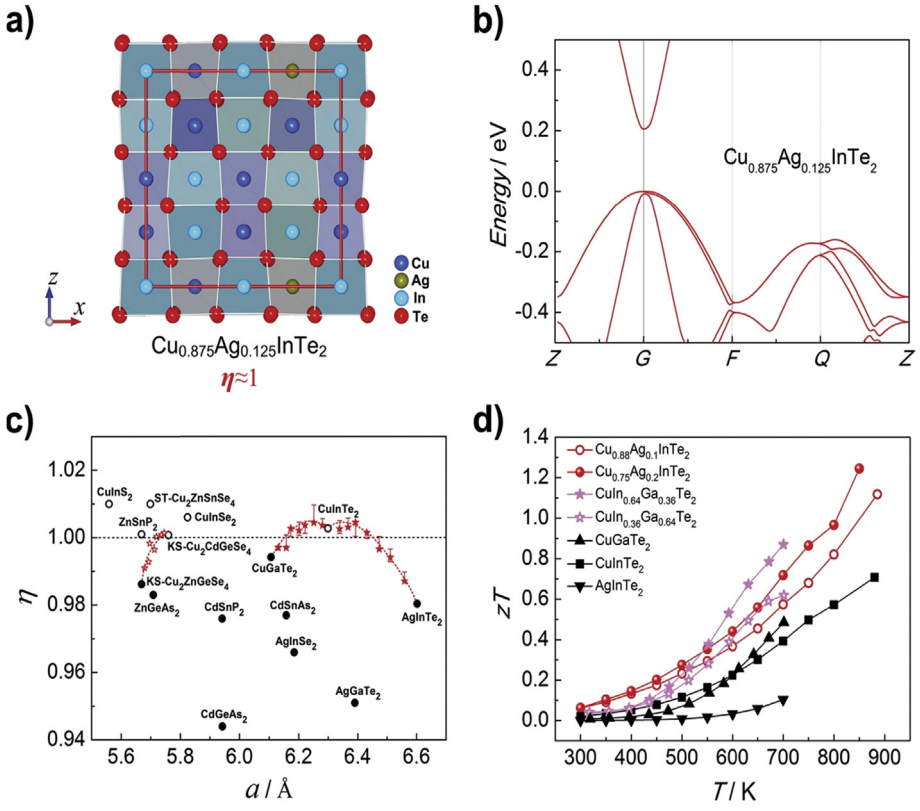

Fig. 2. Crystal structure and electronic bands, η vs. *a* compound map for designing high-performance multinary chalcopyrites, and temperature dependence of *zT* for selected multinary chalcopyrite TE materials. (a) Calculated projected plane representation of the crystal structure on the (010) plane for $Cu_{0.875}Ag_{0.125}InTe_2$. (b) Electronic bands of $Cu_{0.875}Ag_{0.125}InTe_2$. (c) Calculated tetragonal distortion parameter η as a function of the lattice constant *a* in chalcopyrites with $E_g < 1.7$ eV. (d) Temperature dependent *zT* values of $CuInTe_2$, $CuGaTe_2$ [78] ($AgInTe_2$) and their solid solutions [20].

the scope of prospective TE materials especially among non-cubic semiconductors, such as zintl phases.

3.2. Conductive networks in TE materials — filled skutterudites and diamond-like $Cu_2SnS(Se)_3$

The paradigm of PGEC, introduced by Slack in the 1995 [30], requires the simultaneous occurrence of both crystal-like electron transport and glass-like phonon transport in one material, and plays an important role in designing and optimizing high-performance TE materials. Afterwards, the narrow band gap semiconductors with open structures, i.e., the caged and layered structures, become research aspect. These compounds are distinctly different from the convertional TE compounds such as PbTe, Bi_2Te_3 and so on [1,2,13,15], in which all the components contribute to the electrical transport. In these complex TE compounds only part of the framework atoms is responsible for the electrical transport, i.e., the conductive network. This gives a new approach for TE performance designing. Recent researches indicate that the PGEC concept can be realized in caged-free Cu-based diamond-like compounds because there is Cu−X (X=S, Se) bond network in these compounds [29,30]. In this subsection, we present two kinds of special materials, i.e., caged skutterudites and the caged-free Cu_2SnSe_3 diamond-like semiconductors. The conductive networks in the two types of compounds have been identified, based on which the electrical and thermal transport properties have been optimized.

Skutterudite compounds have the body-centered cubic structure with the space group Im3. The binary skutterudite can be written as MX_3 (M=Co, Rh, Ir, and X=P, As, Sb). There are 32 atoms and two large voids in one conventional cell. The structure of $CoSb_3$ is similar to that of the Perovskite structure ($ACoSb_3$) with its A sites unoccupied. The valence band maximum (VBM) is mainly composed of Sb *p* electrons, and only a little contribution of Co *d* electrons. The bands at conduction band minimum (CBM) have three-fold degeneracy, coming from the hybridization of Sb *p* and Co *d* states. The $CoSb_3$ has large carrier mobility and good electric transport properties [30,32], which makes the $CoSb_3$ compounds to be potential excellent TE materials. The large voids in the crystal structures can be filled with impurity atoms, such as alkali metals (AM) [78–81], alkaline earth elements (AE) [82–84], rare earth elements (RE) [85–88], and their combination [89,90]. The filler atoms form weak chemical bonding with the surrounding Sb atoms, and show little effect on the conduction band bottom and transport properties, except tuning the carrier concentrations (See Fig. 3). Fig. 3 indicates that the filler atoms, usually very metallic cations, form ionic bonds with the surrounding Sb atoms, and do not affect the CBM of $CoSb_3$ except for shifting the Fermi level position. Other results [8] show that in real space there are Sb−Sb and Co−Sb bonding network at the same energy windows near CBM, and the filler atom K is totally isolated. The origin comes from the weak interaction between fillers and Sb atoms due to the relatively large crystal voids. There thus exists a conductive

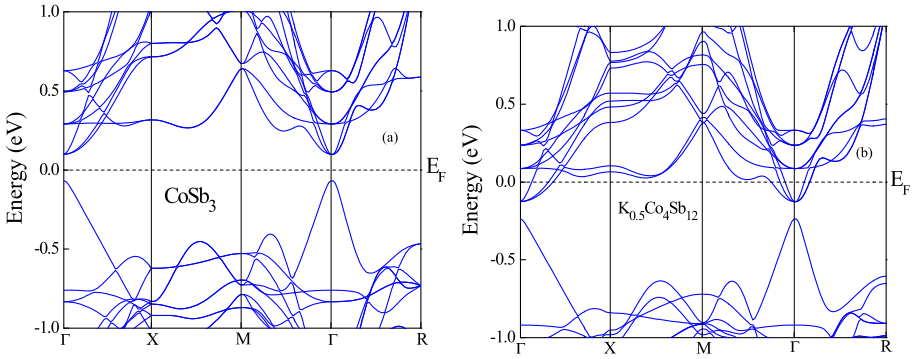

Fig. 3. Band structure of (a) pure $CoSb_3$ and (b) K filled $CoSb_3$ around their Fermi levels (set as zero).

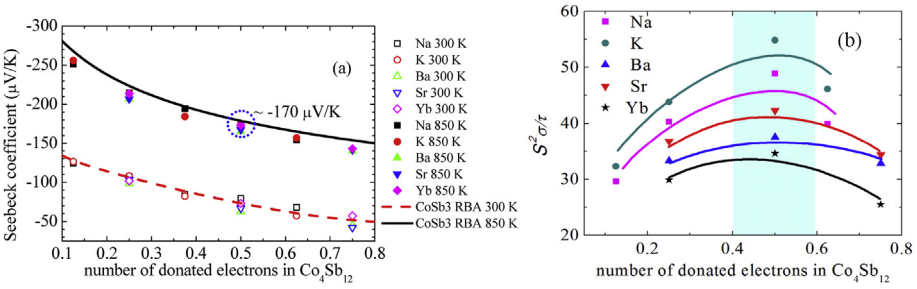

Fig. 4. The Seebeck coefficients (a) and power factors (b) for various n-type filled skutterudites investigated. The RBA results for unfilled Co_4Sb_{12} are also given for comparison. Only the power factor results at 850 K are given in (b) [92].

transport network derived from Sb–Sb and Co–Sb covalent bonding in n-type $CoSb_3$. This is the distinguishing feature for $CoSb_3$ to be likely "electron crystal" materials.

Fig. 4(a) shows the Seebeck coefficients of single-, double-, and multiple-filled $CoSb_3$ as a function of donated electron numbers at 300 K and 850 K, respectively. Fig. 4(b) shows the power factors as a function of donated electron numbers only at 850 K. The theoretical Seebeck coefficients of different fillers (see Fig. 4(a)) follow the same trend predicted by the rigid band approximation (RBA) calculation based on unfilled Co_4Sb_{12} [91,92]. In the experiments, a very similar trend is observed for single-, double-, and even multiple-filled $CoSb_3$ [33]. These results indicate the existence of conductive network in n-type filled $CoSb_3$, and the difference among fillers in terms of electrical transport is only reflected by their different numbers of valence electrons. Interestingly, the power factor reaches the maximum when filling levels reach ~0.5 electrons in the unit of Co_4Sb_{12}. The results agree well with many earlier reports and experimental measurements [33].

The filler atoms introduce the low frequency optic phonons and reduce lattice thermal conductivities. For different filler atoms, the frequencies are different and can be classified into three types, i.e., the low frequencies of RE atoms, the middle ones of AE atoms, and the high ones of AM [93–95]. Combinations of filler atoms with different vibration frequencies can scatter acoustic phonons in a broad frequency range, thus minimizing the lattice thermal conductivities. Combining the optimal rule for electrical transport properties, the independent controlling transport of electrons and phonons can be realized in n-type filled skutterudites. Based on the mentioned theory, high-performance materials can be predicted, such as dual-filled $CoSb_3$, Ba–Ce, Ba–Yb, Sr–Yb, Na–Yb, and multiple-filled Na–Ba-Yb, Ba–La–Yb etc. The high performance materials are indeed obtained via the related experiments on Ba–La–Yb filled skutterudites [21,33,39,93].

For n-type filled skutterudites, the Co-*d* and Sb-*p* electrons compose the band edge structures of CBM, which supply the channels for electronic transport properties. The atoms in filled skutterudites can be classified into two categories, i.e., Co and Sb, forming the strong chemical bonding framework and the conductive network for electrons, and filler atoms, forming only the relatively weak bonding with neighboring Sb atoms. The filler atoms locate out of the conductive network, and they only modulate carrier concentrations. The concept of conductive network is not limited to the caged structures. As long as the material has a strong chemical bonding to stabilize the framework, while the other weak chemical bond can introduce low-frequency vibration modes and optimize the electrical and thermal transport properties, then the PGEC feature may be achieved. It is thus concluded that the PGEC concept can be extended into caged-free compounds.

Cu-based diamond-like compounds are kinds of potential TE materials due to their low thermal conductivity and relatively high mobility [94–97]. Some Cu-based compounds were studied in experiment and show good TE performance, such as $Cu_2Zn(Cd)SnSe_4$, $CuInTe_2$, $Cu_3As(Sb)Se_4$ etc, the figures of merit zT have reached 0.6–0.7 at 700 K [73,98–104]. Recently, our work showed that the character of PGEC could be possibly achieved in Cu_2SnSe_3 [41,42]. We investigated the electronic structures, chemical bonding, and transport properties of ternary Cu_2SnSe_3, and the results indicated that TE performance could be enhanced by using the optimization method mentioned above.

Cu_2SnSe_3 is monoclinic with Cc symmetry below 700 K [105–107]. There are 24 atoms in the unit cell which has the structure of Cu_2SiS_3. Based on the electronic structure results shown in Fig. 5(a), we found that the upper VBs are mainly composed of Cu *d* and Se *p* orbitals and contained no obvious contribution from Sn atoms. Therefore, we expected that p-type doping on Sn sites has little influence on the upper VB shape and only denoted holes. This is expected to be rather important for the TE performance because it provides a site for alloying and doping, while maintaining reasonable mobility. The CBs are composed mainly of Sn *s* and Se *p* states. The CB structure consisting of a single relatively light band is much less favorable for TE performance than the VB structure.

For further charge density distribution analysis, we found that there is a distribution of electronic states on the three-dimensional (3D) [-Cu-Se-Cu-] network in Cu_2SnSe_3, forming an anti-bonding conductive network for hole transport [42]. With Sn-site doping, the band structures closing to VBM

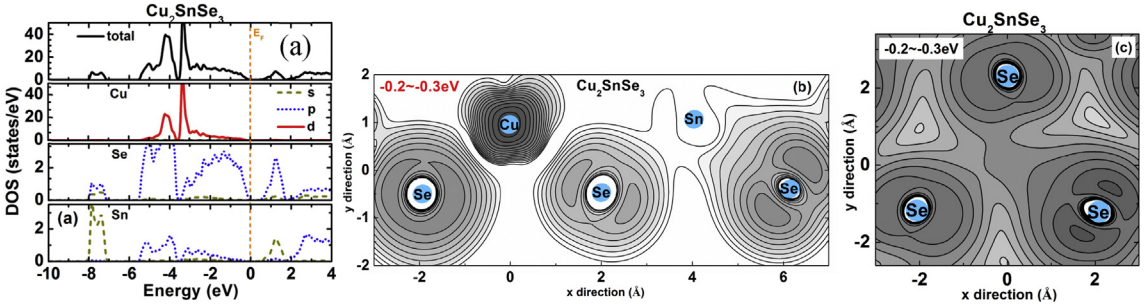

Fig. 5. (a)Total and atom-projected density of states for Cu_2SnSe_3. The Fermi levels are set to zero. (b) Contour plots of the partial charge density in energy windows −0.2~−0.3 eV (indicated in the figures) for Cu_2SnSe_3 on Cu–Se–Sn plane. (c) Contour plots of the partial charge density for the states falling in the energy range of −0.2 eV to −0.3 eV for Cu_2SnSe_3 on the close packed Se–Se–Se plane The contours are logarithmically spaced. The VBM is set to be 0 eV. The contour levels are from −3.3 to 0 with the interval of 0.15 [40].

change slightly except for the shifting of the Fermi levels into upper VB. Based on electron counting, for a doping level of near 10% In substituting for Sn (i.e. near 0.1 holes/cell doping), the Fermi level is the range of −0.2 to −0.3 eV, and thus the corresponding charge density distributions (see Fig. 5(b)) are responsible for hole transport. Clearly these are anti-bonding Cu *d* − Se *p* hybridized states [42]. The Cu_2SnS_3 system shows the similar results as Cu_2SnSe_3 [42]. Furthermore, the closely packed Se framework (the distances between the nearest chalcogen atoms on the planes are only 3.9 Å for Se−Se) may also contributes to hole transport. This is consistent with a recent observation that a relatively rigid Se sublattice is considered to be responsible for hole transport in $Cu_{2-x}Se$ with completely disordering Cu atoms [38]. The overlap of the delocalized *p* states of Se in space (see Fig. 5(c)) forms a delocalized Se−Se conductive path, and contribute to the channel for hole transport [30]. This also favors the large DOS in the upper VB and consequently large Seebeck coefficients in these compounds. These conductive networks give the optimization approach in electronic transport properties [41,42].

The electronic transport properties were studied using the Boltzmann transport theory. Fig. 6(a) shows the calculated Seebeck coefficients as a function of holes in Cu_2SnX_3 (X=S, Se) at 300 K and 700 K by RBA and supercell structures. The solid (red) and dashed (black) lines indicate the results for Cu_2SnSe_3 and Cu_2SnS_3 in RBA, while the symbols show the calculated Seebeck coefficients for the Ga-, In-, and Tl-doped Cu_2SnSe_3 (solid) and Cu_2SnS_3 (open) as obtained by using supercell structures. The supercell approach, as long as the doping level is kept the same, reproduces the RBA results of the Seebeck coefficients very well for Cu_2SnSe_3 at an elevated temperature, indicating the validity of RBA. Fig. 6(b) shows the power factor ($S^2\sigma/\tau$) as a function of carrier concentration at 700 K for Cu_2SnX_3 (X=Se, S) using the RBA approach. The number of holes for achieving the maximum power factors of these compounds can be estimated to be 0.1 per Cu_2SnX_3 formula unit. Experimentally, the 0.1 In substitution for Sn in Cu_2SnSe_3 was carried out, showing the optimized power factor and good TE performance, which agree well with the theoretical results [41,42].

In this subsection, we optimized the TE performance by using the conductive network in caged skutterudites and caged free Cu-based diamond-like compounds. For skutterduites and Cu_2SnSe_3 systems, the Sb−Sb, Co−Sb, and Cu−Se, Se−Se conduction network forming relatively strong chemical bonding and stabilize framework structure, and the position of crystal void in skutterudites and Sn in Cu_2SnSe_3 systems is out of the network. Doping at voids and Sn sites can optimize carrier concentration, and simultaneously reduce the lattice thermal conductivity due to the filler scattering and mass fluctuation respectively, making these two kinds of TE materials exhibit the behavior of PGEC. This work profounds the understanding of PGEC concept, and extends the concept from caged structures to caged free compounds. Compounds with three-dimensional bond network and at least one more selective occupied sites that can be doping are expected as potential candidates for TEs.

Based on the studies above, the concept of conductive network was not limited to the two types of compounds. It could be realized in compounds with hierarchical chemical bonding, that the strong chemical bonding builds up the conductive network and maintain the excellent electrical transport properties. The atoms on the weak bonding, which reduces the lattice thermal conductivity, can be manipulated to tune the carrier concentrations without destroying the conductive network. This concept can be also realized in Cu_2Se, liquid-like Cu_3SbSe_3 etc [38,108]. The Se−Se bonding composites the electron conductive network, while the Cu atoms have the liquid-like behavior that leads to the low thermal conductivity. These workimprove the understanding of the microscopic physical mechanism of transport, which is important in designing novel TE materials.

3.3. High-throughput material screening − thermoelectric half-Heusler as an example

Band engineering and conductive network have been widely adopted to study electrical transport, and the challenge of the theoretical perspective is how to use these band structure engineering to predict and design high-performance TE materials in a large scale. High-throughput computational

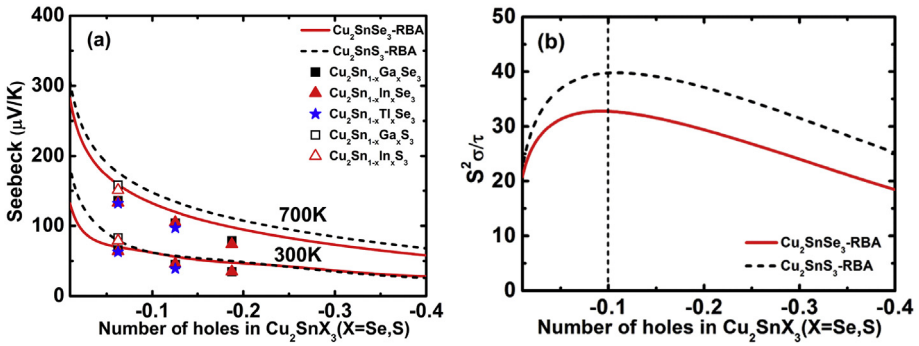

Fig. 6. The Seebeck coefficient (S) and power factor ($S^2\sigma/\tau$) as a function of number of holes in Cu_2SnSe_3 and Cu_2SnS_3. The solid and dashed lines show RBA results for Cu_2SnSe_3 and Cu_2SnS_3, respectively. The symbols (a) are the calculated the Seebeck coefficients for the Ga-, In-, and Tl- doped Cu_2SnX_3 in a supercell approach [40].

materials design is an emerging area in materials science, and have been used in energy conversion materials, such as lithium ion battery and TE materials [43–46,109]. By combining first principles and Boltzmann transport theory, we systematically investigated the electronic structures and TE performance for over 30 HH compositions, and some promising compounds are predicted and several of them are confirmed recently.

Half-Heusler compounds have the general formula ABX, where A and X form a simple rock salt structure with B filled with one of the two body diagonal positions [43]. Ternary HH compounds of the MgAgAs structure type exhibit a variety of interesting physical properties. When the total valence electron counts (VEC) in a primitive HH unit cell is 18, all the constituent atoms complete their electronic shells, and the HH becomes a semiconductor. Fig. 7 shows the crystal structure of a typical HH compound. There are 3 atomic positions, A, B, and X in one primitive unit cell. For thermoelectric HHs, A is usually an early transition (IIIB or IVB) or rare-earth metal, X is a main group element (IVA or VA), and B is normally a transition metal between A and X in the periodic table. Over the years, there have been a few semiconducting HHs investigated as potential thermoelectric materials, with the focus especially on MNiSn, MCoSb (M=Ti, Zr, and Hf) and related isoelectronic alloys [65,110–118]. This is only a very small fraction of compounds that crystallize in HH structure. In fact there are more than 100 HHs that could be found in the Inorganic Crystal Structure Database (ICSD) [119]. Even using the criterion of VEC = 18 for semiconductors, there are still more than 30 HHs left. Using the DFT-based transport calculations discussed above and high throughput screening, the electrical transport properties could be evaluated in order to find new HHs with promising properties. We use the following rules to screen HHs for further detailed investigation [119]. a) VEC equals to 18. Chemical bonding analysis shows that only HHs with 18 valence electrons may be semiconductors, which are suitable for TE purpose. b) The HH compounds with lanthanides, except La, are excluded. Lanthanides contained HHs usually have no gaps, which behave as metals, and therefore possess poor TE properties. Besides, unfilled *f* electrons usually need to be treated by *ab initio* method with strong-correlation effects included. Applying these two rules leads to those HH compounds, which list in Table 1. All the HHs in Table 1 have transition metals on their A, B sites, and thus *d* states are expected to become dominant at VBM and CBM. A-site elements vary from IIIB-VB group, while B-site elements are from Fe subgroup to IB group. Transition metals with different numbers of *d* electrons possess different atomic energy levels at CBM and VBM, and

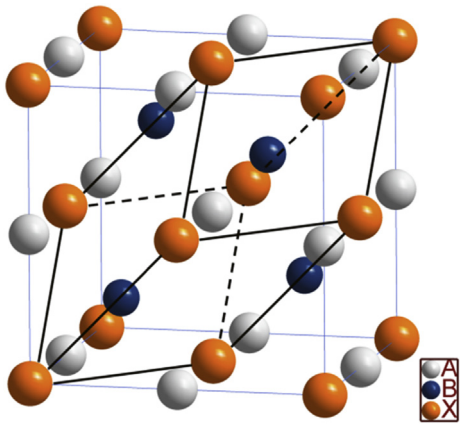

Fig. 7. The crystallographic and primitive unit cell of a typical HH compound ABX.

Table 1
TE transport properties of VEC = 18 HHs. The maximum power factor is in unit of $\tau \times 10^{14}$ W cm^{-1} K^{-2} s^{-1} and the corresponding p- or n-type doping levels are in the unit of (electron/unit cell).

Type	IVB-(Ni, Pd)					IVB-Pt				
Name	TiNiSn	ZrNiSn	HfNiSn	ZrPdSn	HfPdSn	TiPtSn	ZrPtSn	HfPtSn		
Gap (eV)	0.451	0.515	0.396	0.495	0.401	0.830	1.020	0.936		
Max PF(p)	25.13	21.93	22.03	19.62	19.83	24.91	21.11	21.46		
Max PF(n)	14.45	14.43	14.44	12.52	12.78	18.99	12.36	12.34		
p doping	−0.028	−0.019	−0.014	−0.017	−0.013	−0.033	−0.019	−0.014		
n doping	+0.013	+0.009	+0.009	+0.009	+0.008	+0.118	+0.014	+0.013		
Type	IIIB-(Ni, Pd)					IIIB-Pt		IIIB-IB		
Name	ScNiSb	ScNiBi	YNiSb	YNiBi	LaPdBi	YPtSb	ScPtSb	YAuPb	ScAuSn	
gap (eV)	0.281	0.191	0.311	0.219	0.310	0.411	0.685	0.000	0.145	
Max PF(p)	15.82	14.54	13.18	11.98	8.54	12.56	15.90	10.52	18.53	
Max PF(n)	20.64	21.63	22.83	23.44	25.14	21.02	18.58	12.96	13.50	
p doping	−0.006	−0.006	−0.005	−0.004	−0.003	−0.004	−0.007	−0.016	−0.011	
n doping	+0.016	+0.016	+0.017	+0.015	+0.013	+0.034	+0.026	+0.016	+0.009	
Type	IVB-(Co, Rh)					VB-(Co, Rh)		VB-(Fe, Ru)		
Name	TiCoSb	ZrCoBi	TiRhSb	ZrRhSb	HfRhSb	NbCoSn	NbRhSn	VFeSb	NbFeSb	TaRuSb
Gap (eV)	1.05	0.992	0.773	1.215	1.145	0.987	0.665	0.324	0.529	0.655
Max PF(p)	65.95	52.88	21.92	18.51	18.42	67.10	56.12	38.03	35.49	28.79
Max PF(n)	22.57	23.58	10.86	22.51	22.26	24.12	7.85	9.35	7.59	7.08
p doping	−0.157	−0.152	−0.021	−0.012	−0.010	−0.084	−0.202	−0.052	−0.040	−0.025
n doping	+0.195	+0.038	+0.008	+0.121	+0.037	+0.045	+0.002	+0.007	+0.003	+0.003

consequently, determine the band gaps. HHs in Table 1 are classified by their A and B site elements. Band gaps are 0.8–1.2 eV for (IVB, VB)-(Co, Rh)-containing HHs, 0.2–0.3 eV for IIIB-(Ni, Pd), 0.4–0.5 eV for IVB-(Ni, Pd), 0.3–0.7 eV for VB-(Fe, Ru), and 0–0.2 eV for IIIB-IB. Usually cross substitution between elements in the same column at the B sites does not affect the gap value substantially, except for Pt substituting for Ni or Pd (from ZrNiSn, ZrPdSn to ZrPtSn), which gives an enlarged band gap by several tenths of electron volt. Elements at the X sites can be approximately considered as accommodators for the donated valence electrons from atoms at A and B positions, leading to the formation of band gaps, and they themselves do not substantially affect the gap values.

Similar to other TE semiconductors, semiconducting HHs with VEC = 18 need some levels of doping to reach their maximum p-type or n-type power factors. Due to the wide range of dopants and their small amounts in the whole systems, it is very difficult to calculate doped HHs and compare their electrical properties directly. Instead, we adopt the so-called RBA. It is a reasonably good approximation if the doping level is not rather high, and has been widely used for theoretical study of TE materials [43]. The optimal doping level is defined as the integral of DOS from band edge to the energy level position corresponding to the maximum or the peak of power factor (see Fig. 8). For instance, the optimal n-type doping level for ZrNiSn is estimated to be +0.009 e/u.c. This indicates that ZrNiSn reaches its maximum n-type power factor after 0.009 electrons are added per unit cell, which could be achieved by substituting 0.9% Sb for Sn. In Table 1, optimal doping levels and related power factors for every HH are listed. However, we should check the agreements between our calculated data and existing experimental ones before further analysis. Table 2 shows the results. We gave the dopants and the corresponding doping levels for HHs, and for comparison, the optimal doping levels and the corresponding Seebeck coefficients were calculated. For the approximations used above, and the uncertainties in experiment data, the agreement is reasonably and acceptable.

Table 1 shows the information about how to select good HHs from calculations. For p-type materials, the HHs with

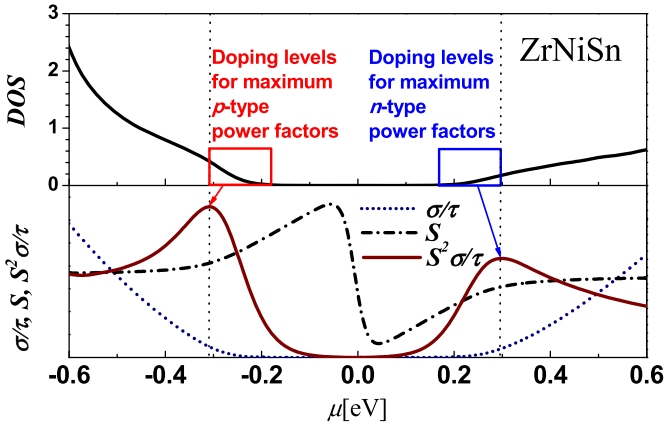

Fig. 8. Procedure of evaluating p- or n-type optimal doping levels [43].

Table 2
Comparisons of theoretical and experimental optimal doping levels, as well as the corresponding Seebeck coefficients at 300 K.

Systems	Experimental doping levels Seebeck (μV/K)	Theoretical doping levels Seebeck (μV/K)
ZrNiSn	1% Sb for Sn [111]	0.9%
n-type	−103	−138
HfPtSn	1% Co or Ir for Pt [114]	1.4%
p-type	120(Co)/130(Ir)	150
TiCoSb	15–30% Fe for Co [117]	15.7%
p-type	153.6	111
NbCoSn	6–10% Sb for Sn [119]	4.5%
n-type	−90	−113
ZrCoSb	10–15% Sn for Sb [118]	7%
p-type	150	129

relatively high power factors usually contain Co, Fe, and Rh. Other IVB and IIIB containing compounds, usually having Ni subgroup and IB group as B-site atoms, are less promising p-type materials. Based on the estimated n-type power factors, IIIB-(Ni, Pd) HHs are expected to have better performance than the IVB-Ni-containing ones (i.e., ZrNiSn) which have been extensively studied in recent years. LaPdBi has the highest n-type power factor. Furthermore, some Co-containing HHs also show reasonable n-type performance. Fig. 9 shows the relationship between the maximum power factor and the corresponding carrier concentration for both p- and n-type HHs. Notice that the best n-type HHs fall in the range of 10^{20}-10^{21} cm^{-3} and the best p-type over 10^{21} cm^{-3}, both correspond to heavily doped semiconductors. These results calculated from realistic and complicated band structures are in reasonable agreement with the optimal carrier concentration estimated based on a simple two-band semiconductor model [120]. Fig. 9 also shows the information that in p-type, high power factors require high carrier concentrations. However, some IIIB-(Ni, Pd) compounds stand out for their n-type power factors, with relatively low carrier concentrations required. Band character analysis shows that *p* states from X-site elements are unneglectable at the CBM of these compounds, which enhances the group velocities of carriers due to the high TDs and good power factors.

A systematical investigation of the electronic structures and electrical transport properties for over 30 well selected HHs is quite interesting. Our work provides an overall picture of the electrical performance of the series compounds [43]. Theoretically, there are still many issues to be solved in predicting the exact values of electrical transport quantities. However, for the compounds with the similar structures, the calculated results are expected to be comparable with each other, and therefore provide a systematic evaluation about their relative performance even with some uncertainties. Through the evaluations of optimal doping levels and corresponding power factors, several HH systems with promising performance are predicted. For p-type, VFeSb, NbFeSb, and the HHs with Co, Fe, and Rh behave relatively high power factors. Recently, Fu et al. investigated the TE performance of Nb(V)FeSb based HH, and they optimized the band effective mass and mobility via a band engineering approach through

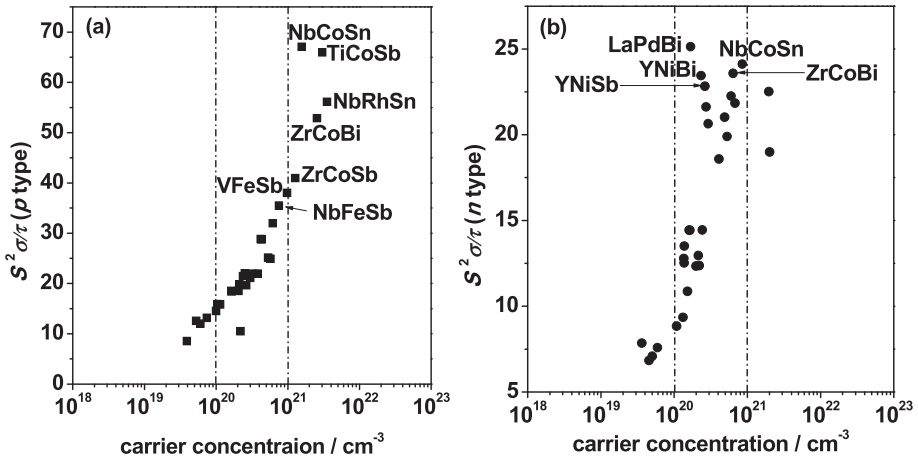

Fig. 9. Maximum power factors vs the corresponding carrier concentrations for (a) p-type and (b) n-type cases. Compound names are indicated in the plots [43].

changing the content of Nb [121,122]. As a result, the highest zT values can reach 1.5 when fully optimized, which are greater than the values of ZrNiSn- and TiCoSb-based HHs, and revoke the research interest on this type of materials. These results verify the theoretical methods shown in the study, which can be easily adopted to large scale high-throughput material screening on electrical transport properties with the help of crystal database.

3.4. Novel thermoelectric transport from spin-orbit-coupling and Rashba effect

As is mentioned above, it is very beneficial for materials with high band degeneracies because it will give the enhanced Seebeck coefficient. In this subsection, we demonstrated a new spin effect that can lead to the alteration of the electronic structures—the Rashba spin splitting. The Rashba effect exists in materials with strong spin-orbit coupling and inversion asymmetry [22–29]. The degeneracy of spin-up and spin-down bands is lifted and the band extrema are shifted aside from the high-symmetric axis, as shown in Fig. 10(a) and (c). The spin-split strength of Rashba effect can be determined by the Rashba parameter α_R, which is associated with Rashba energy, E_0 and momentum shift k_0 by $\alpha_R = 2E_0/k_0$. Due to the structural inversion asymmetry in low-dimensional systems, the nontrivial spin-split phenomena have been investigated in Bi/Ag surface alloy [123], Bi monolayer/quantum film [124,125], and Pt/Si nanowire [126]. More recently, bulk systems with strong Rashba effect have been discovered, including BiTeX (X = I, Br, Cl) [127–129], α-GeTe [130], α-SnTe [131], $LaOBiS_2$ [131,132], and AMX_3 (A=CH_3NH_3, M=Pb, Sn, X=I, Br) [133]. The influence of Rashba effect on the transport properties is fundamentally significant for both spintronics and thermoelectrics.

Dimensionality reduction in DOS has been found in the Rashba systems, originating from the topological change of Fermi surface in low charge density regime [134]. In Fig. 10(b) and (d), DOS is altered across the Dirac point (i.e., Rashba energy E_0), which is one- and two-dimensional-like for quantum wells and bulk materials with the Fermi energy below E_0. The corresponding Fermi surface is an annulus and elliptic torus in the low energy region. The area of the Fermi surface changes with the shifted Fermi energy, leading to the dimensionality reduction in the Rashba systems. This unusual nature reminds us of the low dimensional theory in thermoelectrics. The TE performance of low-dimensional systems should be better than that of the bulk materials, because of the unique DOS [135–137]. We would speculate that the Rashba spin-split systems might have higher TE performance than the usual spin-degenerate systems.

By utilizing the Boltzmann transport theory and relaxation time approximation (relaxation time $\tau(E) = \tau_0 E^r$, τ_0 is a constant and r is the scattering parameter) [138], we can analytically obtian the Seebeck coefficient S and carrier concentration n in the Rashba systems. In two-dimensional Rashba-split quantum wells, due to the one-dimensional DOS, under parabolic band approximation, the S and n have the forms as [139].

$$S_{RSB}^{2D} = \pm\frac{k}{e}\left[\eta - \frac{(r+3/2)F_{r+1/2}(\eta)}{(r+1/2)F_{r-1/2}(\eta)}\right], \tag{5}$$

$$n_{RSB}^{2D} = \frac{m_{ab}^{*}(kTE_0)^{1/2}}{\pi\hbar^2 L_z}F_{-1/2}(\eta), \tag{6}$$

For the bulk Rashba materials, because of the constant DOS, the S and carrier concentration can be expressed as [140].

$$S_{RSB}^{3D} = \pm\frac{k}{e}\left[\eta - \frac{(r+2)F_{r+1}(\eta)}{(r+1)F_r(\eta)}\right], \tag{7}$$

$$n_{RSB}^{3D} = \frac{kT(m^{*})^{3/2}E_0^{1/2}}{2^{1/2}\pi\hbar^3}F_0(\eta). \tag{8}$$

where $\eta = E_F/kT$ denotes the reduced Fermi energy, k is the Boltzmann constant, e is the electron charge, m^* is the effective mass, m_{ab}^* is the in-plane effective mass, and $F_n(\eta)$ is the nth Fermi-Dirac integral $F_n(\eta) = \int_0^\infty \xi^n/[\exp(\xi-\eta)+1]d\xi$.

BiTeI is a bulk material with a giant Rashba effect, which has a Rashba energy E_0 = 0.11 eV, momentum shift

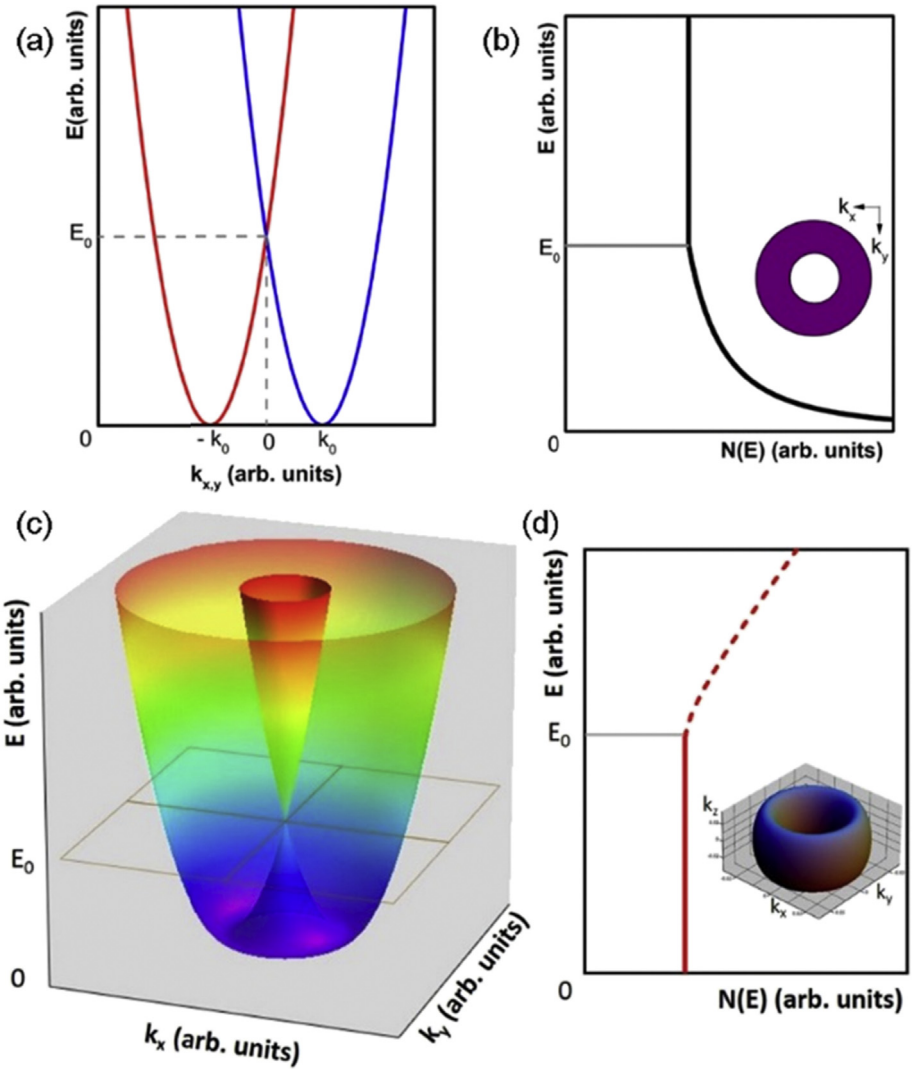

Fig. 10. The band structure and density of states for Rashba spin-split (a, b) quantum wells, (c, d) bulk materials. Insets in (c, d) show the topologies of corresponding Fermi surfaces ($E < E_0$).

$k_0 = 0.05$ Å^{-1}, and Rashba parameter $\alpha_R = 4.3$ eV Å [140,141]. The in-plane and total effective mass are 0.09 and 0.19 m_e, where m_e is the free electron mass [141]. Using a constant relaxation time ($r = 0$), we can numerically calculate the TE properties in Rashba 2D quantum wells and 3D bulk materials through Eqs. (5)–(8), respectively. Fig. 11 shows the carrier concentration dependent S and electrical term S^2n at 300 K, where results for Rashba spin-split band (RSB) and spin-degenerate SPB both are given. For the 2D quantum wells, we take BiTeI (in ab-plane) as the well material and assume the thickness of 2 nm in both RSB and SPB models. As the Fermi energy is shifted from the band bottom up to the Dirac point, it turns out that 2D and 3D systems with RSB have a greater S in the low energy region. The maximum electrical term S^2n can be twice greater than that with SPB, which is a significant enhancement of TE performance. Comparing 2D and 3D systems with the same kind of band model, we found that 2D systems tend to have better S and electrical term at lower carrier concentrations. We also find that a 2.67 nm thick 2D quantum well with SPB and 0.19 m_e effective mass has the same S *versus* n curve of 3D bulk BiTeI [139]. This is due to the 2D-like constant DOS in bulk Rashba systems. The numerically calculated results for 3D RSB are consistent with the experimental data of bulk BiTeI [140]. Meanwhile, the S of 2D Rashba quantum wells is similar to that in quantum wires [139].

In this subsection, general models of TE calculation have been introduced for Rashba spin-split quantum wells and bulk materials. The substantial enhancement of S and electrical term has been found in the 2D and 3D Rashba systems. The Fermi energy can be lowered in these systems for given carrier concentrations due to the unique low-dimensional DOS. Thus, the transport distribution function can be strengthened, leading to higher S. Our work may stimulate more efforts on exploring TE properties in the Rashba spin-split systems.

4. Conclusions and outlook

This paper presented several methods for TE performance optimization and designing in some materials from band

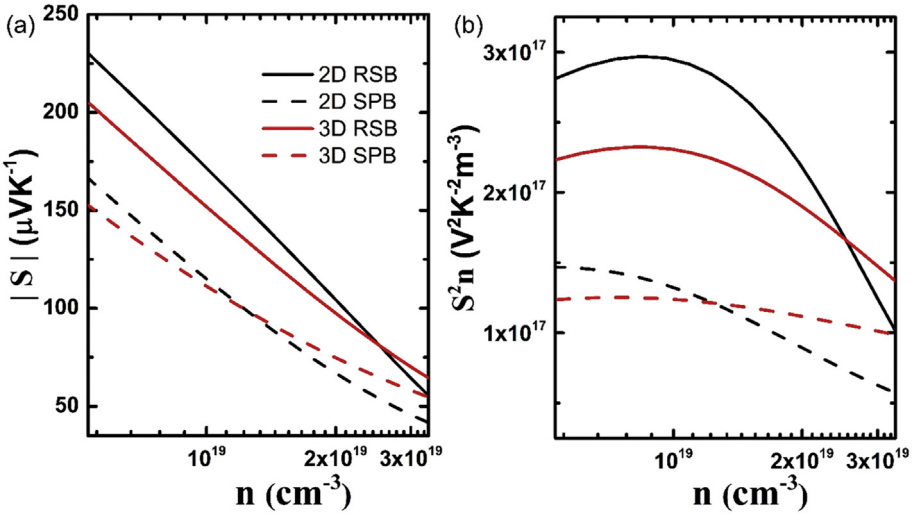

Fig. 11. Carrier concentration dependent S and electrical term S^2n in 2D quantum wells and 3D bulk systems. RSB and SPB denote the Rashba spin-split band and spin-degenerate single parabolic band, respectively.

engineering. For non-cubic compounds, we introduced a unity-η rule to select high-performance non-cubic TE materials. This strategy could make cubic-like degenerate electronic bands through the utilization of a rational pseudocubic structure and broaden the scope of prospective TE materials. By individually controlling the transport properties of electrons and phonons, filled skutterudites presented features of PGEC and good TE performance. For Cu-based diamond-like compounds, we proposed the 3D bond network to stabilize the framework, and one more selective sites, Sn sites, which donated electrons to complete the electron shells, reside in the framework formed by Cu−Se bond in Cu_2SnSe_3. This work could makes an extension to the PGEC family and pave an effective way for the further study of these diamond-like compounds with different bond network. In high-throughput calculations, we applied 18 VEC rule to filter good candidates from a large database HH compounds, using the combination of electronic structures and the Boltzmann transport theory. Some of the top-ranked candidates were confirmed by recent experiments. At last, we enhanced electrical transport by a new effect, i.e., the Rashba spin splitting effect. For materials with the Rashba effect, which required strong spin-orbit coupling and inversion asymmetry, the degeneracy of spin-up and spin-down bands was split and the band extreme were shifted aside from the high-symmetric axis.

Focusing on the above mentioned TE materials, including HH, caged skutterudite $CoSb_3$, and diamond-like semiconductors, we developed several rules for structure modification and performance optimization. Based on that, we could have a deeper understanding of the mechanism of the collective electrical and thermal transport, identify the scientific fundamentals of the PGEC concept, and provide guidance for TE performance optimization as well as novel TE materials designing. These are the important parts of TE materials and physics, the TE performance is closely related to electrical and thermal transport properties. There are still many problems in completely controlling the electrical and thermal transport mechanisms, which need further study.

For electrical transport, by studying the electronic structures and transport properties, we could have the basic understanding on the relationship between macro-structure symmetry and microscope band degeneracy. The simple rule applies to the pseudocubic structure compounds, and give the direction to search for high-performance TE materials. For compounds with other structure, such as layered structures, this simple rule is inappropriate and a more universal parameter is needed to modify the electronic structures and then the transport properties. Recently, a simple yet successful strategy has been adopted to discover and design high-performance layered TE materials through minimizing the crystal field splitting energy of orbitals to realize high orbital degeneracy, and the approach could be extended to several other non-cubic materials [21]. Besides the band degeneracy, the spin split in electronic structures also has an effect on the transport properties, such as the Rashba effect [139,140]. The Rashba effect will lead to the dimensionality reduction, which enhances the DOSs and S in the 2D and 3D Rashba systems. The other spin-entropy enhancement could be widespread in the transition-metal oxides [142,143], such as $NaCoO_2$, the spin state of Co could be changed as the content of oxygen. Even the controlling mechanism is not clear, the S is likely to be dominated by spin entropy terms, indicating that this could be a promising class of materials to search for the improved TE materials.

Development of new mechanism for band engineering is urgent for optimizing and designing novel high-performance TE materials. The concept of conductive network provides a new approach for the enhancement of TE performance. We used this concept to optimize TE performance in filled skutterudites and Cu-based diamond-like compounds. Several qualitative descriptions have already been provided in ‘conductive network’ [8,41,42]. At the present, we examine and identify the conductive network mainly based on the density of states or charge density at the energy window

responsible for the electrical transport. These could not be sufficient to quantify the contributions to the electrical transport. A more accurate and definitive of the contribution to electrical transport properties is needed. The type of work is interesting but challenging, and will be investigated in the future work.

High-throughput computational screening of TE materials will accelerate the screening and designing of new high-performance TE materials. So far, most high-throughput work focus on simple structure compounds, such as HHs, by using the Boltzmann transport theory for electrical transport or anharmonic interatomic force constant for thermal transport. For more complex TE materials, in additional to the direct transport calculations, the implementations of simple yet powerful selection rule, i.e., the unity η rule, are crucial. Generally speaking, using the advanced selection rule relating to the properties is more efficient, and can even speed up the high-throughput screening for functional materials [20,21]. The other direction for the improvement of high-throughput work can be the implementation of the scattering term in the algorithm. The high-throughput work usually neglects the influence from the carrier or phonon scattering on the transport properties for the simplicity reason. In fact, the relaxation times for both carriers and phonons are able to calculate explicitly. In order to improve the accuracy of high-throughput work, the development of simplified algorithm regarding the scattering terms is necessary.

Thermal transport properties are also complicated because the mechanism of phonon scattering is diversified. Recently some compounds with part-crystalline part-liquid have attracted great attention because of their ultralow thermal conductivities and unique lattice dynamic behaviors, such as Cu_3SbSe_3 [144], Cu_2Se [38], etc. Recent work well described the variation law of lattice thermal conductivity for part-crystalline system by introducing local vibration similar like that of disorder atoms, and the results agree well with the existing experiments [108]. This work demonstrates the theoretical challenge of correctly describing phonon and thermal transports in complex materials, and the models can be used in materials with chemical-bond hierarchy. These results imply the complexity of phonon scattering mechanisms in compounds with chemical bond hierarchy. More advanced theoretical models counting for the large structural fluctuations in these compounds are needed in the future.

Finally, we reviewed several topics regarding the band engineering in TE materials, and pointed out several directions for the future theoretical work. More efforts need to be paid to dig through these directions, as well as other theoretical topics, which could favor the TE research.

Acknowledgment

This work was supported by National Basic Research Program (973-program) of China under Project No. 2013CB632501, and NSFC Grants (11234012, 51572167, 51121064, 11574333), Shanghai Municipal Science and Technology Commission (Grant No. 14DZ2261200, 15DZ2260300, and 15JC1400301), and the Key Research Program of Chinese Academy of Sciences (Grant No. KGZD-EW-T06). Jiong Yang acknowledges support by the Program for Professor of Special Appointment (Eastern Scholar) at Shanghai Institutions of Higher Learning.

References

[1] Goldsmid HJ, Douglas RW. The use of semiconductors in thermoelectric refrigeration. J Appl Phys 1954;5:386–90.
[2] Goldsmid HJ. Thermoelectric refrigeration. New York: Plenum; 1964.
[3] Sales BC. Thermoelectric materials. Smaller is cooler. Science 2002; 295:1248–9.
[4] Poudel B, Hao Q, Ma Y, Lan YC, Minnich A, Yu B, et al. High-thermoelectric performance of nanostructured bismuth antimony telluride bulk alloys. Science 2008;320:634–8.
[5] Abelson RD. In: Rowe DW, editor. Thermoelectrics handbook. Boca Raton: CRC Press; 2006. p. 1–26. ch.56.
[6] Bell LE. Cooling, heating, generating power, and recovering waste heat with thermoelectric systems. Science 2008;321:1457–61.
[7] Kraemer D, Poudel B, Feng HP, Caylor JC, Yu B, Yan X, et al. High-performance flat-panel solar thermoelectric generators with high thermal concentration. Nat Mater 2011;10:532–8.
[8] Yang J, Xi LL, Qiu WJ, Wu LH, Shi X, Chen LD, et al. Band engineering and rational design of high performance thermoelectric materials from first-principles. NPJ Comput Mater 2016;2:15015.
[9] Singh DJ, Mazin II . Calculated thermoelectric properties of La-filled skutterudites. Phys Rev B 1997;56:R1650–3.
[10] Mecholsky NA, Resca L, Pegg IL, Fornari M. Theory of band warping and its effects on thermoelectronic transport properties. Phys Rev B 2014;89:155131.
[11] Parker D, Chen X, Singh DJ. High three-dimensional thermoelectric performance from low-dimensional bands. Phys Rev Lett 2013;110: 146601.
[12] Shirai K, Yamanaka K. Mechanism behind the high thermoelectric power factor of $SrTiO_3$ by calculating the transport coefficients. J Appl Phys 2013;113:053705.
[13] Heremans JP, Jovovic V, Toberer ES, Saramat A, Kurosaki K, Charoenphakdee A, et al. Enhancement of thermoelectric efficiency in PbTe by distortion of the electronic density of states. Science 2008;321: 554–7.
[14] Pei YZ, Wang H, Snyder GJ. Band engineering of Thermoelectric Materials. Adv Mater, 201;24:6125.
[15] Pei YZ, Shi X, LaLonde A, Wang H, Chen LD, Snyder GJ. Convergence of electronic bands for high performance bulk thermoelectrics. Nature 2011;473:66.
[16] Heremans JP, Wiendlocha B, Chamoire AM. Resonant levels in bulk thermoelectric semiconductors. Energy Environ Sci 2012;5:5510–30.
[17] Liu W, Tan Xj, Yin K, Liu HJ, Tang XF, Shi J, et al. Convergence of conduction bands as a means of enhancing thermoelectric performance of n-type Mg2Si1−xSnx solid solutions. Phys Rev Lett 2012;108: 166601.
[18] Tan GJ, Shi FY, Hao SQ, Chi H, Bailey TP, Zhao LD, et al. Valence band modification and high thermoelectric performance in SnTe heavily alloyed with MnTe. J Am Chem Soc 2015;137:11507–16.
[19] Li W, Chen ZW, Lin SQ, Chang YJ, Ge BH, Chen Y, et al. Band and scattering tuning for high performance thermoelectric Sn1−xMnxTe alloys. J Materiomics 2015;1:307–15.
[20] Zhang JW, Liu RH, Cheng N, Zhang YB, Yang JH, Uher C, et al. High-performance pseudocubic thermoelectric materials from non-cubic chalcopyrite compounds. Adv Mater 2014;26:3848–53.
[21] Zhang JW, Song LR, Madsen GKH, Fischer KFF, Zhang WQ, Shi X, et al. Designing high-performance layered thermoelectric materials through orbital engineering. Nat Commun 2016;7:10892.
[22] Rashba EI. Symmetry of bands in wurzite-type crystals. 1. Symmetry of bands disregarding spin-orbit interaction. Sov Phys Solid State 1959;1: 368–80.
[23] Rashba EI. A method of experimental examination of possibility of introduction of universal surface recombination rate during

investigation of the photoelectric processes kinetics. Sov Phys Solid State 1960;2:1109−22.
[24] Bychkov YA, Rashba EI. Properties of a 2D electron gas with lifted spectral degeneracy. JETP Lett 1984;39:78−81.
[25] Mori K, Sakakibara H, Usui H, Kuroki K. Pudding-mold type band in a potential thermoelectric material $CuAlO_2$: comparison with $NaxCoO_2$. Phys Rev B 2013;88:075141.
[26] Usui H, Kuroki K, Nakano S, Kudo K, Nohara M. Pudding-mold-type band as an origin of the large Seebeck coefficient coexisting with metallic conductivity in carrier-doped $FeAs_2$ and $PtSe_2$. J Electron Mater 2014;43:1656−61.
[27] Kuroki K, Arita R. "Pudding mold" band drives large thermopower in $NaxCoO_2$. J Phys Soc Jpn 2007;76:083707.
[28] Shi HL, Parker D, Du MH, Singh DJ. Connecting thermoelectric performance and topological-insulator behavior: Bi_2Te_3 and Bi_2Te_2Se from first principles. Phys. Rev. Appl 2015;3:014004.
[29] Xiao C, Li DP, Ma ZS. Unconventional thermoelectric behaviors and enhancement of figure of merit in Rashba spintronic systems. Phys Rev B 2016;93:075150.
[30] Slack GA. CRC handbook of thermoelectrics. Florida: CRC Press; 1995. p. 407−40.
[31] Nolas GS, Poon JK. Recent developments in bulk thermoelectric materials. Mater Res Soc Bull 2006;31:199−205.
[32] Uher C. Thermoelectric materials research I. In: Tritt T, editor. Semiconductors and semimetals series 69. Elsevier; 2001. p. 139−253.
[33] Shi X, Yang J, Salvador JR, Chi MF, Cho JY, Wang H, et al. Multiple-filled skutterudites: high thermoelectric figure of merit through separately optimizing electrical and thermal transports. J Am Chem Soc 2011;133:7837−46.
[34] Nolas GS, Morelli DT, Tritt TM. Skutterusites: a phonon-glass-electron crystal approach to advanced thermoelectric energy conversion applications. Annu Rev Mater Sci 1999;29:89−116.
[35] Tang YL, Chen S-W, Snyder GJ. Temperature dependent solubility of Yb in Yb−$CoSb_3$ skutterudite and its effect on preparation, optimization and lifetime of thermoelectric. J Materiomics 2015;1:75−84.
[36] Duan B, Yang J, Salvador JR, He Y, Zhao B, Wang SY, et al. Electronegative guests in $CoSb_3$. Energy Environ Sci 2016. http://dx.doi.org/10.1039/c6ee00322b.
[37] Kauzlarich SM, Brown SR, Snyder GJ. Zintl phases for thermoelectric devices. Dalton Trans 2007:2099−107.
[38] Liu HL, Shi X, Xu FF, Zhang LL, Zhang WQ, Chen LD, et al. Copper ion in liquid-like thermoelectrics. Nat Mater 2012;11:422−5.
[39] Shi X, Kong H, Li C-P, Uher C, Yang JH, Salvador JR, et al. Low thermal conductivity and high thermoelectric figure of merit in n-type BaxYbyCo4Sb12 double-filled skutterudites. Appl Phys Lett 2008;92:182101.
[40] Xi LL, Yang J, Shi X, Zhang WQ, Chen LD, Yang JH. Sci. Sin. Filled skutterudites: from single to multiple filling (in Chinese). Phys Mech Astron 2011;41:706−28.
[41] Shi XY, Xi LL, Fan J, Zhang WQ, Chen LD. Cu-Se bond network and thermoelectric compounds with complex diamondlike structure. Chem Mater 2010;22:6029−31.
[42] Xi LL, Zhang YB, Shi XY, Yang J, Shi X, Chen LD, et al. Chemical bonding, conductive network, and thermoelectric performance of the ternary semiconductors Cu_2SnX_3 (X = Se, S) from first principles. Phys Rev B 2012;86:155201.
[43] Yang J, Li HM, Wu T, Zhang WQ, Chen LD, Yang JH. Evaluation of half-Heusler compounds as thermoelectric materials based on the calculated electrical transport properties. Adv Funct Mater 2008;18:2880.
[44] Wang SD, Wang Z, Setyawan WY, Mingo N, Curtarolo S. Assessing the thermoelectric properties of sintered compounds via high-throughput ab-initio calculations. Phys Rev X 2011;1:021012.
[45] Carrete J, Li W, Mingo N, Wang S, Curtarolo S. Finding unprecedentedly low-thermal-conductivity half-Heusler semiconductors via high-throughput materials modeling. Phys Rev X 2014;4:011019. Carrete J, Mingo N, Wang S, Curtarolo S. Nanograined Half-Heusler Semiconductors as Advanced Thermoelectrics: An Ab Initio High-Throughput Statistical Study. Adv Funct Mater 2014;24:7427−7432.
[46] Zhu H, Hautier G, Aydemir U, Gibbs ZM, Li GD, Bajaj S, et al. Computational and experimental investigation of $TmAgTe_2$ and XYZ_2 compounds, a new group of thermoelectric materials identified by firstprinciples high-throughput screening. J Mater Chem C 2015;3:10554.
[47] Blöchl PE. Projector augmented-wave method. Phys Rev B 1994;50:17953.
[48] Kresse G, Joubert D. From ultrasoft pseudopotentials to the projector augmented-wave method. Phys Rev B 1758;1999:59.
[49] Kresse G, Furthmüller J. Efficient iterative schemes for ab initio total-energy calculations using a plane-wave basis set. Phys Rev B 1996;54:11169.
[50] Paier J, Marsman M, Hummer K, Kresse G, Gerber IC, Angyan JG. Screened hybrid density functionals applied to solids. J Chem Phys 2006;124:154709.
[51] Perdew JP, Burke K, Ernzerhof M. Generalized gradient approximation made simple. Phys Rev Lett 1996;77:3865.
[52] Zhang YK, Yang WT. Comment on "generalized gradient approximation made simple". Phys Rev Lett 1998;80:890.
[53] Hammer B, Hansen LB, Nørskov JK. Improved adsorption energetics within density-functional theory using revised Perdew-Burke-Ernzerhof functionals. Phys Rev B 1999;59:7413.
[54] Zhang YB, Yuan X, Sun XD, Shih B-C, Zhang PH, Zhang WQ. Comparative study of structural and electronic properties of Cu-based multinary semiconductors. Phys Rev B 2011;84:075127.
[55] Zhang YB, Zhang JW, Gao WW, Abtew TA, Wang YW, Zhang PH, et al. Near-edge band structures and band gaps of Cu-based semiconductors predicted by the modified Becke-Johnson potential plus an on-site Coulomb U. J Chem Phys 2013;139:184706.
[56] Ziman JM. Electrons and phonons: the theory of transport phenomena in solids. London: Oxford University Press; 1960.
[57] Scheidemantel TJ, Ambrosch-Draxl C, Thonhauser T, Badding JV, Sofo JO. Transport coefficients from first-principles calculations. Phys Rev B 2003;68:125210.
[58] Madsen GKH. Automated search for new thermoelectric materials: the case of LiZnSb. J Am Chem Soc 2006;128:12140.
[59] Madsen GKH, Singh DJ. BoltzTraP-A code for calculating band-structure dependent quantities. Comput Phys Commun 2006;175:67.
[60] Parker D, Singh DJ. High-temperature thermoelectric performance of heavily doped PbSe. Phys Rev B 2010;82:035204.
[61] Madsen GKH, Schwarz K, Blaha P, Singh DJ. High-temperature thermoelectric performance of heavily doped PbSe. Phys Rev B 2003;68:125212.
[62] Chaput L, Pécheur P, Tobola J, Scherrer H. Transport in doped skutterudites: ab initio electronic structure calculations. Phys Rev B 2005;72:085126.
[63] Johnsen A, Bentien A, Madsen GHK, Nygren M, Iversen BB. Crystal structure and transport properties of nickel containing germanium clathrates. Phys Rev B 2007;76:245126.
[64] Wang H, Pei Y, LaLonde AD, Snyder GJ. Heavily doped p-type PbSe with high thermoelectric performance: an alternative for PbTe. Adv Mat 2011;23:1366.
[65] Uher C, Yang J, Hu S, Morelli DT, Meisner GP. Transport properties of pure and doped MNiSn (M=Zr, Hf). Phys Rev B 1999;59:8615.
[66] Nag BR. Theory of electrical transport in semiconductors. Oxford: Pergamon Press; 1972.
[67] http://www.mgi.shu.edu.cn/Portals/675/transoptic.zip.
[68] Singh DJ. Theoretical and computational approaches for identifying and optimizing novel thermoelectric materials. In: Tritt TM, editor. Recent trends in thermoelectric materials research II; 2001. p. 125−78.
[69] Rowe J, Shay J. Extension of the quasicubic model to ternary chalcopyrite crystals. Phys Rev B 1971;3:451.
[70] Artus L, Bertrand Y, Ance C. Crystal-field and spin-orbit interactions at the fundamental gap of $AgGaSe_2$ chalcopyrite compound. J Phys C Solid State Phys 1986;19:5937.

[71] Plirdpring T, Kurosaki K, Kosuga A, Day T, Firdosy S, Ravi V, et al. Chalcopyrite $CuGaTe_2$: a high-efficiency bulk thermoelectric material. Adv Mater 2012;24:3622. You have full text access to this content.

[72] Ibanez M, Zamani R, LaLonde A, Cadavid D, Li W, Shavel A, et al. $Cu_2ZnGeSe_4$ nanocrystals: synthesis and thermoelectric properties. J Am Chem Soc 2012;134:4060–3.

[73] Kosuga A, Plirdpring T, Higashine R, Matsuzawa M, Kurosaki K, Yamanaka S. High-temperature thermoelectric properties of $Cu_{1-x}InTe_2$ with a chalcopyrite structure. Appl Phys Lett 2012;100:042108.

[74] Liu RH, Xi LL, Liu HL, Shi X, Zhang WQ, Chen LD. Ternary compound $CuInTe_2$: a promising thermoelectric material with diamond-like structure. Chem Commun 2012;48:3818–20.

[75] Ying PZ, Zhou H, Gao YL, Li YY, Li YP, Lian XL, et al. Thermoelectric properties of a wide–gap chalcopyrite compound $AgInSe_2$. Key Eng Mater 2012;519:188–92.

[76] Yusufu A, Kurosaki K, Kosuga A, Sugahara T, Ohishi Y, Muta H, et al. Thermoelectric properties of $Ag_{1-x}GaTe_2$ with chalcopyrite structure. Appl Phys Lett 2011;99:061902.

[77] Li YP, Meng QS, Deng Y, Zhou H, Gao YL, Li YY, et al. High thermoelectric performance of solid solutions $CuGa_{1-x}In_xTe_2$ ($x = 0–1.0$). Appl Phys Lett 2012;100:231903.

[78] Pei YZ, Chen LD, Zhang WQ, Shi X, Bai SQ, Zhao XY, et al. Synthesis and thermoelectric properties of KyCo4Sb12. Appl Phys Lett 2006;89:221107.

[79] Pei YZ, Yang J, Chen LD, Zhang WQ, Salvador JR, Yang JH. Improving thermoelectric performance of caged compounds through light-element filling. Appl Phys Lett 2009;95:042101.

[80] Zhang WQ, Shi X, Mei ZG, Xu Y, Chen LD, Yang J, et al. Predication of an ultrahigh filling fraction for K in $CoSb_3$. Appl Phys Lett 2006;89:112105.

[81] Mei ZG, Yang J, Pei YZ, Zhang WQ, Chen LD. Alkali-metal-filled $CoSb_3$ skutterudites as thermoelectric materials: theoretical study. Phys Rev B 2008;77:045202.

[82] Chen LD, Kawahara T, Tang XF, Goto T, Hirai T, Dyck JS, et al. Anomalous barium filling fraction and n-type thermoelectric performance of BayCo4Sb12. J Appl Phys 2001;90:1864.

[83] Zhao XY, Shi X, Chen LD, Zhang WQ, Pei YZ. Synthesis and thermoelectric properties of Sr-filled skutterudite SryCo4Sb12. J Appl Phys 2006;99:053711.

[84] Puyet M, Lenoir B, Dauscher A, Dehmas M, Stiewe C, Muller E. High temperature transport properties of partially filled CaxCo4Sb12 skutterudites. J Appl Phys 2004;95:4852. Puyet M, Dauscher A, Lenoir B, Dehmas M, Stiewe C, Muller E, et al., Beneficial effect of Ni substitution on the thermoelectric properties in partially filled Cay-Co4−xNixSb12 skutterudites. J Appl Phys 2005;97:083712.

[85] Morelli DT, Meisner GP, Chen BX, Hu SQ, Uher C. Cerium filling and doping of cobalt triantimonide. Phys Rev B 1997;56:7376.

[86] Kuznetsov VL, Kuznetsova LA, Rowe DM. Effect of partial void filling on the transport properties of $Nd_xCo_4Sb_{12}$ skutterudites. J Phys Condens Matter 2003;15:5035.

[87] Pei YZ, Bai SQ, Zhao XY, Zhang WQ, Chen LD. Thermoelectric properties of $Eu_yCo_4Sb_{12}$ filled skutterudites. Solid State Sci 2008;10:1422.

[88] Nolas GS, Kaeser M, Littleton RTIV, Tritt TM. High figure of merit in partially filled ytterbium skutterudite materials. Appl Phys Lett 2000;77:1855.

[89] Xi LL, Yang J, Zhang WQ, Chen LD, Yang JH. Anomalous dual-element filling in partially filled skutterudites. J Am Chem Soc 2009;131:5560–3.

[90] Xi LL, Yang J, Lu CF, Mei ZG, Zhang WQ, Chen LD. Systematic study of the multiple-element filling in caged skutterudite $CoSb_3$. Chem Mater 2010;22:2384–94.

[91] Yang J, Shi X, Zhang WQ, Chen LD, Yang JH. In: Rowe DW, editor. Thermoelectrics handbook. Boca Raton: CRC Press; 2012. p. 1–24. ch.9.

[92] Yang J, Xi LL, Zhang WQ, Chen LD, Yang JH. Electrical transport properties of filled $CoSb_3$ skutterudites: a theoretical study. J Electron Mater 2009;38:1397.

[93] Yang JH, Zhang WQ, Bai SQ, Mei ZG, Chen LD. Dual-frequency resonant phonon scattering in $Ba_xR_yCo_4Sb_{12}$ (R=LaR=La, Ce, and Sr). Appl Phys Lett 2007;90:192111.

[94] Berger LI. Semiconductor materials. Boca Raton: CRC Press; 1997. p. 264.

[95] Kim JH, Seong D, Ihm GH, Rhee C. Measurement of the thermal conductivity of Si and GaAs wafers using the photothermal displacement technique. Inter J Thermophys 1998;19:281.

[96] Pauling L. The nature of the chemical bond. 3rd ed. Ithaca, New York: Cornell University Press; 1960. p. 93.

[97] Allred AL. Electronegativity values from thermochemical data. J Inorg Nucl Chem 1961;17:215.

[98] Shi XY, Huang FQ, Liu ML, Chen LD. Thermoelectric properties of tetrahedrally bonded wide-gap stannite compounds Cu2ZnSn1−xInxSe4. Appl Phys Lett 2009;94:122103.

[99] Liu ML, Chen IW, Huang FQ, Chen LD. Improved thermoelectric properties of Cu-Doped quaternary chalcogenides of $Cu_2CdSnSe_4$. Adv Mater 2009;21:3808–12.

[100] Liu ML, Huang FQ, Chen LD, Chen IW. A wide-band-gap pp-type thermoelectric material based on quaternary chalcogenides of Cu_2ZnSnQ_4(Q=S,Se). Appl Phys Lett 2009;94:202103.

[101] Skoug EJ, Cain JD, Morelli DT. High thermoelectric figure of merit in the Cu_3SbSe_4-Cu_3SbS_4 solid solution. Appl Phys Lett 2011;98:261911.

[102] Parker D, Singh DJ. Thermoelectric properties of $AgGaTe_2$ and related chalcopyrite structure materials. Phys Rev B 2012;85:125209.

[103] Skoug E, Cain J, Majsztrik P, Kirkham M, Lara-Curzio E, Morelli D. Doping effects on the thermoelectric properties of Cu_3SbSe_4. Sci Adv Mater 2011;3:602.

[104] Cho JY, Shi X, Salvador JR, Yang JH, Wang H. Thermoelectric properties of ternary diamondlike semiconductors Cu2Ge1+xSe3. J Appl Phys 2010;108:073713.

[105] Marcano G, Rincon C, Chalbaud de LM, Bracho DB, Perez GS. Crystal growth and structure, electrical, and optical characterization of the semiconductor Cu_2SnSe_3. J Appl Phys 2001;90:1847.

[106] Delgado GE, Mora AJ, Marcano G, Rincon C. Crystal structure refinement of the semiconducting compound Cu_2SnSe_3 from X-ray powder diffraction data. Mater Res Bull 2003;38:1949–55.

[107] Onoda M, Chen XA, Sato A, Wada H. Crystal structure and twinning of monoclinic Cu_2SnS_3. Mater Res Bull 1999;35:1563–70.

[108] Qiu WJ, Xi LL, Wei P, Ke XZ, Yang JH, Zhang WQ. Part-crystalline part-liquid state and rattling-like thermal damping in materials with chemical-bond hierarchy. PNAS 2014;111:15031–5.

[109] Kirklin S, Meredig B, Wolverton C. High-throughput computational screening of new Li-ion battery anode materials. Adv Energy Mater 2012;3:252–62.

[110] Shen Q, Chen LD, Goto T, Hirai T, Yang JH, Meisner GP, et al. Effects of partial substitution of Ni by Pd on the thermoelectric properties of ZrNiSn-based half-Heusler compounds. Appl Phys Lett 2011;79:4165.

[111] Bhattacharya B, Tritt TM, Xia Y, Ponnambalam V, Poon SJ, Thadhani N. Grain structure effects on the lattice thermal conductivity of Ti-based half-Heusler alloys. Appl Phys.Lett 2002;81:43–5.

[112] Sakurada S, Shutoh N. Effect of Ti substitution on the thermoelectric properties of (Zr,Hf)NiSn half-Heusler compounds. Grain structure effects on the lattice thermal conductivity of Ti-based half-Heusler alloys. Appl Phys Lett 2005;86:082105.

[113] Kimura Y, Zama A. Thermoelectric properties of p-type half-Heusler compound HfPtSn and improvement for high-performance by Ir and Co additions. Appl Phys Lett 2006;89:172110.

[114] Nolas GS, Sharp J, Goldsmid HJ. Thermoelectrics: basic principles and new materials developments. Berlin: Springer; 2001.

[115] Mastronardi K, Yong D, Wang CC, Khalifah P, Cava RJ, Ramirez AZ. Antimonides with the half-Heusler structure: new thermoelectric materials. Appl Phys Lett 1999;74:1415.

[116] Wu T, Jiang W, Li XY, Zhou YF, Chen LD. Thermoelectric properties of p-type Fe-doped TiCoSb half-Heusler compounds. J Appl Phys 2007;102:103705.

[117] Sekimoto T, Kurosaki K, Muta H, Yamanaka S. High-thermoelectric figure of merit realized in p-type half-Heusler compounds: $ZrCoSnxSb_{1-x}$. J Appl Phys Jpn 2006;46:L673.

[118] Ono Y, Inayama S, Adachi H, Kajitani T. Thermoelectric properties of doped half-Heuslers $NbCoSn_{1-x}Sb_x$ and $Nb_{0.99}Ti_{0.01}CoSn_{1-x}Sb_x$. Jpn J Appl Phys 2006;45:8740.
[119] Inorganic Crystal Structure Database (ICSD). http://icsd.ill.eu/icsd/.
[120] Ioffe AF. Thermoelements and thermoelectric cooling. London, UK: Infosearch; 1956.
[121] Fu CG, Zhu TJ, Liu YT, Xie HH, Zhao XB. Band engineering of high performance p-type FeNbSb based half-Heusler thermoelectricmaterials for figure of merit zT >1. Energy Environ Sci 2015;8:216.
[122] Fu CG, Bai SQ, Liu YT, Tang YS, Xie HH, Chen LD, et al. Realizing high figure of merit in heavy-band p-type half-Heusler thermoelectric materials. Nat Commun 2015;6:8144.
[123] Ast CR, Henk J, Ernst A, Moreschini L, Falub MC, Pacilé D, et al. Giant spin splitting through surface alloying. Phys Rev Lett 2007;98:186807.
[124] Gierz I, Suzuki T, Frantzeskakis E, Pons S, Ostanin S, Ernst A, et al. Silicon surface with giant spin splitting. Phys Rev Lett 2009;103:046803.
[125] Mathias S, Ruffing A, Deicke F, Wiesenmayer M, Sakar I, Bihlmayer G, et al. Quantum-well-induced giant spin-orbit splitting. Phys Rev Lett 2010;104:066802.
[126] Park J, Jung SW, Jung M-C, Yamane H, Kosugi N, Yeom HW. Self-assembled nanowires with giant Rashba split bands. Phys Rev Lett 2013;110:036801.
[127] Ishizaka K, Bahramy MS, Murakawa H, Sakano M, Shimojima T, Sonobe T, et al. Giant Rashba-type spin splitting in bulk BiTeI. Nat Mater 2011;10:521–6.
[128] Eremeev SV, Nechaev IA, Koroteev YM, Echenique PM, Chulkov EV. Ideal two-dimensional electron systems with a giant Rashba-type spin splitting in real materials: surfaces of bismuth tellurohalides. Phys Rev Lett 2012;108:246802.
[129] Sakano M, Bahramy MS, Katayama A, Shimojima T, Murakawa H, Kaneko Y, et al. Strongly spin-orbit coupled two-dimensional electron gas emerging near the surface of polar semiconductors. Phys Rev Lett 2013;110:107204.
[130] Sante DDi, Barone P, Bertacco R, Picozzi S. Electric control of the giant Rashba effect in bulk GeTe. Adv Mater 2013;25:509–13.
[131] Zhang X, Liu Q, Luo J-W, Freeman A, Zunger A. Hidden spin polarization in inversion-symmetric bulk crystals. Nat Phys 2014;10:387.
[132] Liu Q, Guo Y, Freeman AJ. Tunable Rashba effect in two-dimensional $LaOBiS_2$ films: ultrathin candidates for spin field effect transistors. Nano Lett 2013;13:5264–70.
[133] Kim M, Im J, Freeman AJ, Ihm J, Jin H. Switchable S = 1/2 and J = 1/2 Rashba bands in ferroelectric halide perovskites. Proc Natl Acad Sci U S. A 2014;111:6900–4.
[134] Cappelluti E, Grimaldi C, Marsiglio F. Topological change of the Fermi surface in low-density Rashba gases: application to superconductivity. Phys Rev Lett 2007;98:167002.
[135] Hicks LD, Dresselhaus MS. Effect of quantum-well structures on the thermoelectric figure of merit. Phys Rev B 1993;47:12727–31.
[136] Hicks LD, Dresselhaus MS. Thermoelectric figure of merit of a one-dimensional conductor. Phys Rev B 1993;47:16631–4.
[137] Dresselhaus MS, Chen G, Tang MY, Yang RG, Lee H, Wang DZ, et al. New directions for low-dimensional thermoelectric materials. Adv Mater 2007;19:1043–53.
[138] Goldsmid HJ. Introduction to thermoelectricity. Berlin-Heidelberg, Germany: Springer-Verlag; 2009.
[139] Wu LH, Yang J, Wang SY, Wei P, Yang JH, Zhang WQ, et al. Thermopower enhancement in quantum wells with the Rashba effect. Appl Phys Lett 2014;105:202115.
[140] Wu LH, Yang J, Wang SY, Wei P, Yang JH, Zhang WQ, et al. Two-dimensional thermoelectrics with Rashba spin-split bands in bulk BiTeI. Phys Rev B 2014;90:195210.
[141] Bahramy MS, Arita R, Nagaosa N. Origin of giant bulk Rashba splitting: application to BiTeI. Phys Rev B 2011;84:041202.
[142] Wang YY, Rogado NS, Cava RJ, Ong NP. Spin entropy as the likely source of enhanced thermopower in $Na_xCo_2O_4$. Nature 2003;423:425–8.
[143] Singh DJ. Electronic structure of $NaCo_2O_4$. Phys Rev B 2000;61:13397–402.
[144] Skoug EJ, Morelli DT. Role of lone-pair electrons in producing minimum thermal conductivity in nitrogen-group chalcogenide compounds. Phys Rev Lett 2011;107:235901.

Dr. Lili Xi, Shanghai Institute of Ceramics, Chinese Academy of Sciences, China. Email: lilyxi2006@mail.sic.ac.cn. She received B.S. from Sichuan University (2005), China; Ph. D. from Shanghai Institute of Ceramics, Chinese Academy of Sciences (2010), China. After graduated from SICCAS, she was an assistant research in SICCAS, China. Her research was focused on first-principles study on filling fraction of Skutterudites and novel thermoelectric materials.

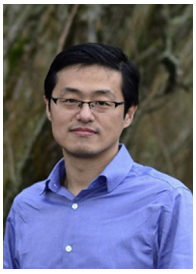

Prof. Jiong Yang, Materials Genome Institute, Shanghai University, China. Email: jiongy@t.shu.edu.cn. He received his Ph. D. from Shanghai Institute of Ceramics, Chinese Academy of Sciences, where he worked for two years after graduation. He was a postdoctoral follow in University of Washington, USA, before the current job title as a professor in Shanghai University. The research focus of Prof. Jiong Yang is on the theoretical understanding of the electron and phonon transport in semiconductors, as well as optimization and design of novel thermoelectric materials.

Prof. Wenqing Zhang, Materials Genome Institute, Shanghai University, China. Email: wqzhang@t.shu.edu.cn. He received his Ph.D. in Shanghai Institute of optics and fine mechanics academy of sciences, Chinese Academy of Sciences (1992), China. He moved to Institute of Physics University of Michigan (USA) as a postdoctor in Physics department from 1993 to 1995. Then he joined the University of Science and Technology Beijing, Harvard University, Princeton University, and Santa Barbara UC University from 1995 to 2004. From 2004 to 2012, he worked in SICCAS as a Cheung Kong Scholar, then he came to Nanjing University from 2012 to 2014. From 2014, he came back to Materials Genome Institute, Shanghai University as the college subdecanal and his current research focuses on computer materials science and materials design on energy conversion materials. He has over 100 peer-reviewed publications papers. His recent awards include APS Fellow (2014), Second Prize of National Natural Science Award of China (2013), Shanghai Natural Science Prize (2012), Pacesetter engineering experts (2009), the National outstanding youth (2008).